PAPER

Check for updates

Degradation of sulfadiazine in aqueous media by peroxymonosulfate activated with biochar-supported ZnFe₂O₄ in combination with visible light in an internal loop-lift reactor†

Yan Wang, [ID] Tao Gan, Jingyu Xiu, Ganghua Liu and Haiming Zou

Solid waste resource utilization and the treatment of wastewater are two important aspects in environmental protection. Here, biochar (BC) derived from municipal sewage sludge has been combined with $ZnFe_2O_4$ to form the photocatalyst $ZnFe_2O_4$/biochar (ZnFe/BC), and it was used to degrade sulfadiazine (SDZ) in the presence of peroxymonosulfate (PMS) under visible (Vis) light irradiation in an internal loop-airlift reactor (ALR). The surface morphology and structure of ZnFe/BC have been characterized by X-ray diffraction (XRD), scanning electron microscopy equipped with an attachment for energy-dispersive spectroscopy (SEM-EDS), X-ray photoelectron spectroscopy (XPS), and UV-Vis diffuse reflectance spectroscopy (UV-Vis DRS). ZnFe/BC displays outstanding photocatalytic performance and reusability. After four reuse cycles of ZnFe/BC in the Vis/ZnFe/BC/PMS system, the SDZ degradation rate and efficiency still reached 0.082 min^{-1} and 99.05%, respectively. Reactive species in this system included free radicals $SO_4^{\bullet-}$, $^{\bullet}OH$, and $^{\bullet}O_2^{-}$, as well as non-radicals $^1O_2$, e^-, and h^+, as established from the results of chemical quenching experiments and electron paramagnetic resonance (EPR) analyses. Moreover, a mechanism of action of the Vis/ZnFe/BC/PMS system for SDZ degradation was proposed. The acute toxicity of the reaction solution towards *Photobacterium phosphoreum* T3 spp. in the Vis/ZnFe/BC/PMS process increased during the first 40 min and then decreased, illustrating that Vis/ZnFe/BC/PMS provided an effective and safe method for the removal of SDZ.

1. Introduction

With the rapid development of the social economy and increase of peoples' quality of life, sulfonamide antibiotics have been used globally to cure infectious diseases in humans as well as in farmed livestock and poultry as a food supplement.[1–3] However, these antibiotics cannot be completely decomposed by animals or humans and are released to the environment through excretion, causing serious harm to the ecosystem due to their chronic toxicity and broad-spectrum antibacterial properties.[2–4] SDZ, as a typical antibiotic, has been widely used and is frequently detected in environmental media.[5,6] Moreover, it is difficult to effectively degrade SDZ by traditional biological methods due to its good solubility and persistence in the aquatic environment.[6] Thus, an effective treatment method is required to treat SDZ-contaminated wastewater before it is released to municipal wastewater treatment plants (WWTPs).

Department of Environmental Science and Engineering, Anhui Science and Technology University, Donghua Road 9#, Fengyang, 233100, China. E-mail: wangyanht@163. com

† Electronic supplementary information (ESI) available. See https://doi.org/10.1039/d2ra04573g

Sulfate radical ($SO_4^{\bullet-}$)-based advanced oxidation processes (SR-AOPs) represent effective treatment or detoxification methods for wastewater contaminated with refractory organics.[7–10] This is because $SO_4^{\bullet-}$ has high average redox potential, good solubility, wide pH flexibility, and a long half-life.[6,10–14] PMS, as a source of $SO_4^{\bullet-}$ in SR-AOPs, has been advantageously applied in the remediation of wastewater due to its ease of storage and convenient transportation. PMS may be activated by transition metal ions,[15] ultraviolet light,[14,16–18] heat,[19] metal oxides,[20–22] or carbonate-rich materials,[23–28] to produce highly reactive species, such as $SO_4^{\bullet-}$ and hydroxyl radicals ($^{\bullet}OH$).

Among these activation methods, heterogeneous photocatalytic systems constitute an effective approach for improving the degradation of recalcitrant pollutants due to their low negative impact on water quality and excellent separation of the catalyst from wastewater, such that a synergistic effect has been observed by some researchers.[29–31] $ZnFe_2O_4$, as a typical representative of bimetallic oxides, has attracted widespread interest because of the natural abundances and nontoxicity of its constituent metals, as well as its high theoretical specific capacitance, narrow band gap, and desirable optical structure, which permit its use as a photocatalyst.[32–34] However, the

application of pure $ZnFe_2O_4$ is limited by its low valence-band (VB) potential, rapid recombination of charge carriers, and aggregation.[35–37] Some carbon-based materials have been employed to overcome these bottlenecks, which show excellent activity due to their high conductivity, large surface area, and better charge separation.[21,38,39] Graphene and carbon nanotubes have been used as support materials, but their practical applications are limited by their complicated preparation processes.[21] Meanwhile, BC is finding increasing applications as a support material and adsorbent due to its simple preparation process and low cost.[40–43] In addition, oxygen-containing functional groups on the surface of BC, such as –COOH and C–OH, can activate PMS to generate reactive species.[42,43] However, we are not aware of any previous report on visible-light irradiation enhanced BC-supported $ZnFe_2O_4$ for PMS activation (Vis/ZnFe/BC/PMS).

In the present study, SDZ was selected as a target antibiotic to assess the enhancing effect of combining PMS with visible light irradiation and ZnFe/BC in ALR. Compared with a mechanically stirred batch reactor or a bubble column reactor, the ALR can provide better mixing, high gas–liquid–solid mass transfer, and low shear stress, resulting in its extensive application in chemical engineering and biotechnology.[44,45] Therefore, the primary objectives of this study were to test the catalytic ability and efficiency of ZnFe/BC for PMS activation and to delineate the reaction mechanism of the Vis/ZnFe/BC/PMS system for the degradation of SDZ in an ALR. Finally, the acute toxicity of the reaction effluent was analyzed.

2. Materials and methods

2.1. Materials

SDZ ($C_{10}H_9N_4NaO_2S$, >98%), 2,2,6,6-tetramethyl-4-piperidinol (TMP), and 5,5-dimethyl-1-pyrrolidine N-oxide (DMPO) were purchased from Aladdin Industrial Corporation (Shanghai, China). PMS ($KHSO_5 \cdot 0.5KHSO_4 \cdot 0.5K_2SO_4$, 4.5% active oxygen) was purchased from Macklin Industrial Corporation (Shanghai, China). Ethanol (EtOH), *tert*-butyl alcohol (TBA), potassium dichromate ($K_2Cr_2O_7$), ethylenediamine tetraacetic acid (EDTA), 1,4-benzoquinone (BQ), iron chloride ($FeCl_3$), sodium azide (NaN_3), acetonitrile (C_2H_3N), formic acid (CH_2O_2), and zinc chloride ($ZnCl_2$) were supplied by Sinopharm Chemical Reagent Co., Ltd. (Shanghai, China). All chemicals were of analytical grade or better and were used as received. All solutions were prepared with deionized water. Dewatered sewage sludge was collected from a municipal wastewater treatment plant in Chuzhou, China.

2.2. Preparation of BC and ZnFe/BC

BC was fabricated by directly calcining drying sewage sludge powder. Dewatered sewage sludge was firstly dried in an oven at 80 °C. It was then smashed and sifted through an 80 mesh sieve. Finally, the sludge powder was transferred into a ceramic boat and was pyrolyzed at 500 °C for 2 h in a tubular reactor (SK-G04123K, China) in N_2 atmosphere.

ZnFe/BC was synthesized by a hydrothermal method.[46,47] BC (1 g) was fully dispersed in deionized water (80 mL) in a beaker with the aid of ultrasonication. $ZnCl_2$ (10 mmol) and $FeCl_3$ (20 mmol) were then added and the mixture was stirred for 100 rpm by means of a mechanical agitator (Eurostar 20 Digital, IKA RW20, Germany) for 20 min. Thereafter, NaOH (1 g) was added to the mixture, which converted it into a brown suspension. This brown suspension was stirred for 10 min and then poured into a 100 mL Teflon-lined stainless steel autoclave. The autoclave was covered and placed in an oven at 180 °C for 24 h. After allowing the autoclave to cool to room temperature, the obtained precipitate was washed several times with deionized water, and then dried at 80 °C for 12 h. The obtained ZnFe/BC was stored in a sample bottle prior to use.

2.3. Experimental procedures

All experiments were performed in an ALR containing 30 mg L^{-1} SDZ solution (1.5 L) at room temperature (25 °C) under irradiation from a lamp. The detailed structure and dimensions of the ALR (Fig. S1†) have been described in a previous report.[48] The requisite compressed gas was injected continuously (40 mL min^{-1}) for 10 min before the experiment from the bottom of the ALR to circulate the catalyst particles throughout the reactor. An Xe lamp with a cut-off filter ($\geq$400 nm) (Heraeus-6, 300 W, providing simulated solar light) was fixed inside a cylindrical Pyrex tube. The Xe lamp was turned on for 30 min before starting the experiment to stabilize its radiation. The requisite amounts of ZnFe/BC and PMS were then added to the ALR, which was taken as $t = 0$ with regard to the reaction time. Aliquots (1 mL) were withdrawn at certain intervals, filtered through a 0.22 μm membrane, and immediately quenched reaction with 20 μL EtOH prior to analysis.

2.4. Analytical methods

The residual SDZ concentration was determined by high-performance liquid chromatography (HPLC, LC-20AB). The HPLC system was equipped with an SPDM20A chromatograph, an LC-20AB pump, and an SPD-10A UV/Vis detector set at a wavelength of 265 nm. A shim-pack VP-ODS C18 column (4.6 mm × 250 mm, 5 μm) was used for separation. The mobile phase was a mixture of acetonitrile and 0.1% (v/v) aqueous formic acid (30 : 70, v/v) and the flow rate was set at 1 mL min^{-1}. The degradation efficiency (R) of SDZ was calculated according to eqn (1):

$$R\ (\%) = (1 - C/C_0) \times 100 \tag{1}$$

where C_0 and C refer to the SDZ concentrations at time 0 and t min. The total organic carbon (TOC) was measured using a Shimadzu TOC analyzer (TOC-L series, Shimadzu, Japan).

The morphologies of the catalysts were inspected with SEM-EDS (Hitachi S-3000N, Japan). The XRD patterns of BC and ZnFe/BC were collected on a D8 Advance spectrometer (Bruker, Germany) operated at 40 kV and 30 mA, employing Cu-K$_\alpha$ radiation ($\lambda = 1.5406$ Å). The surface chemical state was

assessed by XPS (Thermo Fisher, USA) with a monochromated Al-K_α X-ray source. Diffuse reflectance spectra were collected on a UV visible spectrophotometer (UV 3600, Shimadzu, Japan) equipped with a diffuse reflectance measurement accessory and $BaSO_4$ was used as a reflectance standard.

The active species generated in the Vis/PMS, Vis/BC/PMS, and Vis/ZnFe/BC/PMS systems were identified by EPR on an A300-10/12 spectrometer (Bruker, Germany) with a microwave bridge (modulation amplitude 2 G, microwave power 20 mW, modulation frequency 100 kHz). Metal ions (Zn^{2+} and Fe^{3+}) leaching from the catalyst were quantified by atomic absorption spectrometry (ZEEnit 700, Germany).

2.5. Acute toxicity assay

Active toxicities were determined towards luminescent bacteria based on the Chinese standard for water quality determination of acute toxicity (GB/T 15441-1995). Each test was carried out in six replicates.

Freeze-dried powder of *Photobacterium phosphoreum* T3 spp. was purchased from the Institute of Soil Science, Chinese Academy of Sciences (Nanjing, China) and was reconstituted with 3% NaCl solution prior to testing.[49] The variation of luminescence was detected using a Toxicity Determinator (DXY-3, Institute of Soil Science, Chinese Academy of Sciences, Nanjing, China). In a blank test, the effluent of SDZ degradation

was replaced by deionized water. The toxicity was characterized by the percentage inhibition of luminosity (X) according to the following equation (eqn (2)):

$$X\ (\%) = \left(1 - \frac{\text{luminosity of the sample}}{\text{luminosity of the CK}}\right) \times 100 \qquad (2)$$
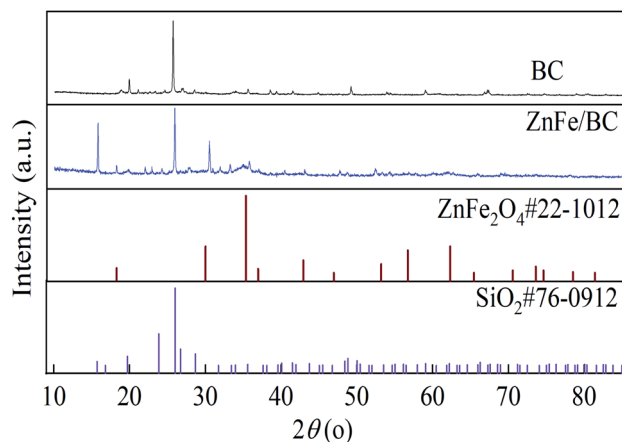
where CK denotes the blank sample.
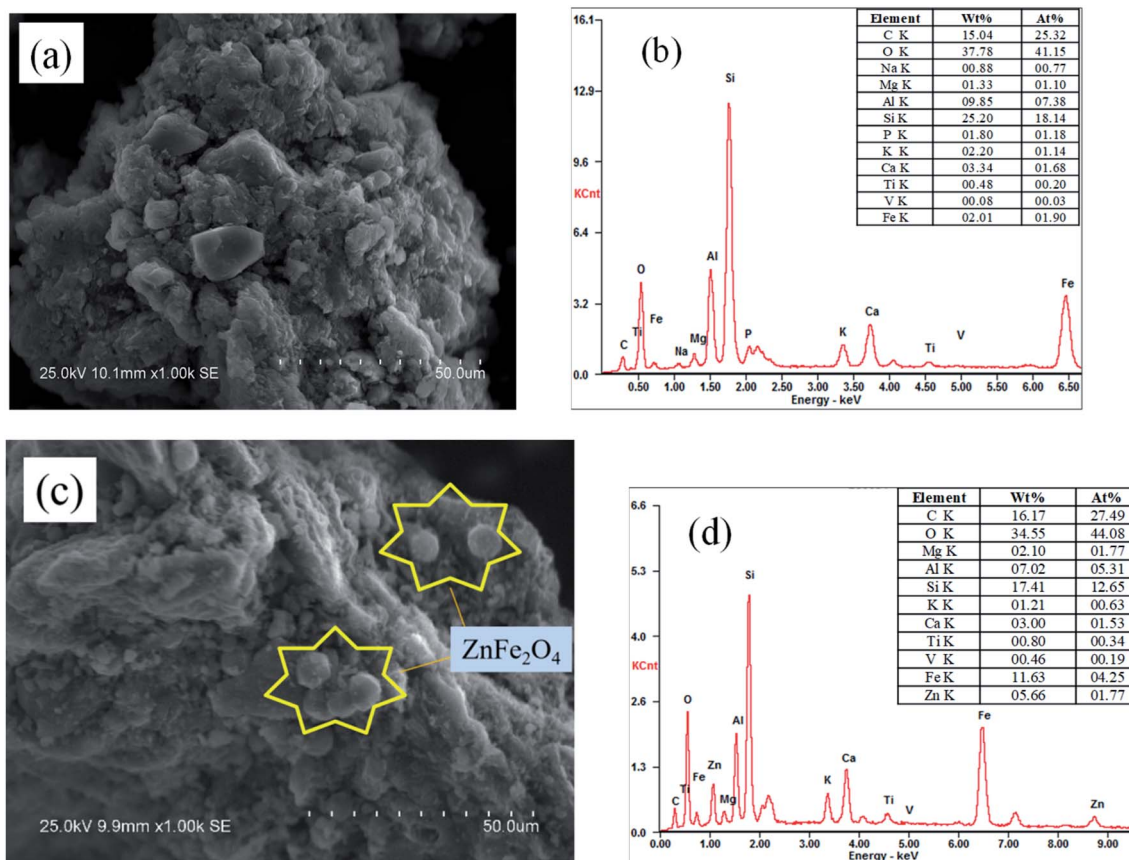

Fig. 2   XRD patterns of BC and ZnFe/BC.

Fig. 1   SEM images of (a) BC and (c) ZnFe/BC, EDS spectrum of (b) BC and (d) ZnFe/BC.

3. Results and discussion

3.1. Characterization of catalysts

The morphologies and elemental compositions of BC and ZnFe/BC were determined by SEM-EDS, and the results are shown in Fig. 1a–c. As shown in Fig. 1a and b, BC obtained from sewage sludge by calcination exhibited a rough surface, with C, O, and Si as its main elements. Fig. 1c reveals many spherical particles on the surface of ZnFe/BC such as the yellow mark, and Fig. 1d

shows the atomic ratio of Zn to Fe to be approximately 1 : 2, suggesting that these spherical particles may consist of $ZnFe_2O_4$.

XRD spectral data shown in Fig. 2 were used to further confirm the crystallinity of the synthesized catalysts. The XRD peaks of BC at 19.73°, 23.86°, 26.03°, 26.72°, and 28.69° corresponded to the (111), (200), (201), (210), and (211) planes and are consistent with the standard reference file of SiO_2 (JCPDS card no. 76-0912). Besides the obvious peak of BC at 26.03°,
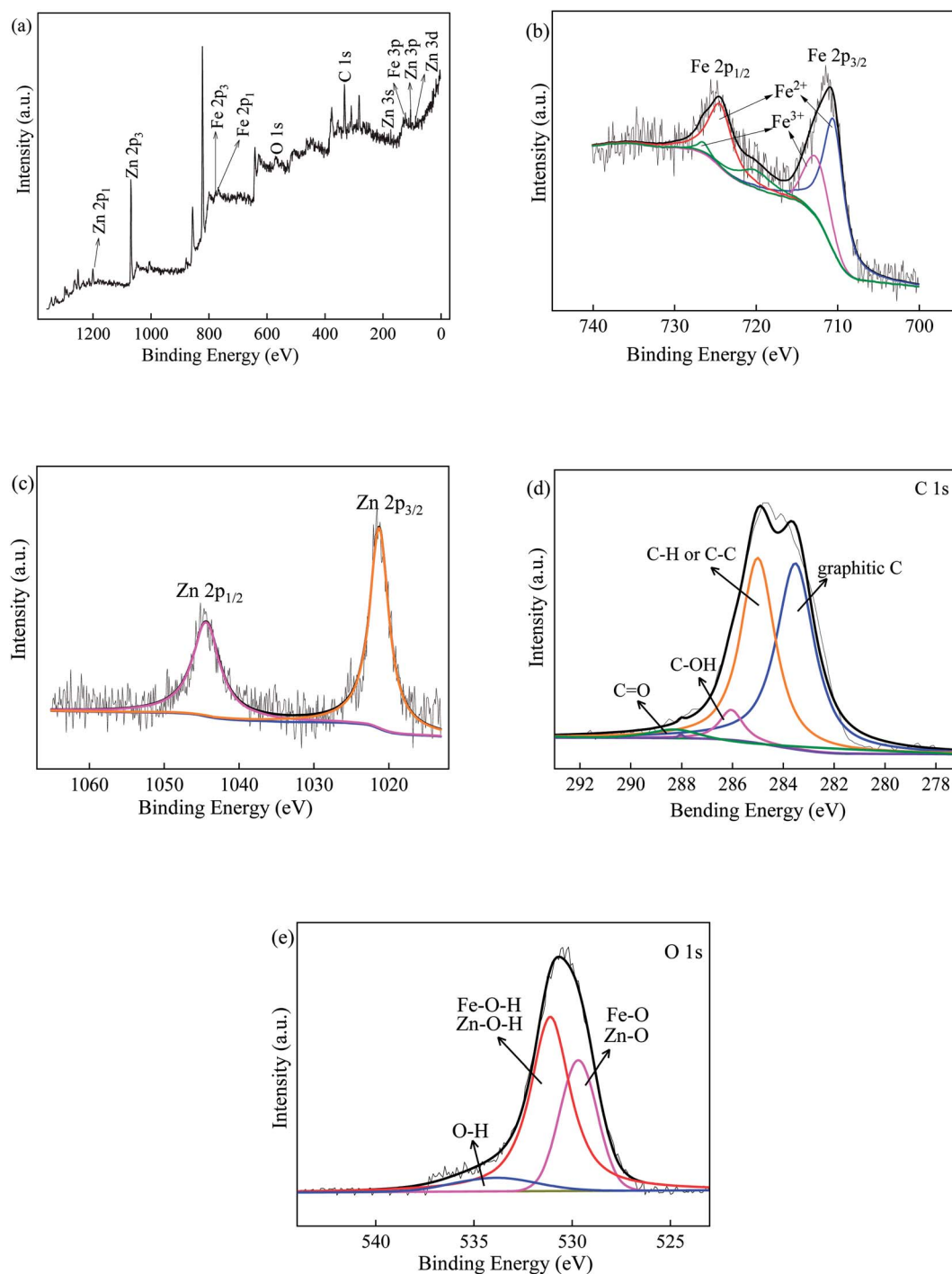

Fig. 3 XPS profile of ZnFe/BC: (a) survey and core spectra of (b) Fe, (c) Zn, (d) C and (e) O.

ZnFe/BC also displayed a well-defined crystal structure, with peaks at 29.92°, 35.26°, 42.88°, 56.63°, and 62.12° attributable to the (220), (311), (400), (511), and (440) planes of spinel $ZnFe_2O_4$ (JCPDS card no. 22-1012).[50,51] Overall, the main component on the surface of BC was $ZnFe_2O_4$, consistent with the SEM-EDS results.

XPS was employed to further interpret the chemical state of the prepared ZnFe/BC sample, and the results are shown in Fig. 3. As can be seen from the survey spectrum in Fig. 3a, the binding energy peaks for the different electronic states confirmed the presence of Zn, Fe, C, and O. The two characteristic Fe 2p peaks seen in Fig. 3b at 711.2 and 724.5 eV corresponded to Fe 2p3/2 and Fe 2p1/2, respectively.[32,51] Interestingly, the two deconvoluted Fe 2p peaks could be resolved to the Fe^{3+} state at binding energies of 710.5 and 726.5 eV and the Fe^{2+} state at 712.6 and 724.4 eV. The satellite peak at 720.1 eV also stemmed from the Fe^{3+} state.[32] The Zn 2p spectrum of ZnFe/BC in Fig. 3c features two peaks at 1021.8 eV and 1044.9 eV, attributable to Zn 2p3/2 and Zn 2p1/2, as expected for Zn^{2+}.[33,52] Fig. 3d shows the C 1s spectrum of ZnFe/BC, which could be deconvoluted into four peaks at 283.5, 285.0, 286.1, and 288.0 eV, attributable to graphitic C, C–H or C–C, C–OH, and C=O, respectively.[33,53] The O 1s spectrum is depicted in Fig. 3e and could be deconvoluted into three peaks at 529.7, 531.5, and 532.6 eV, reflecting the presence of Fe–O/Zn–O, Fe–OH/Zn–OH, and –OH.[32,54] The presence of these elements in their respective states corroborated the formation of $ZnFe_2O_4$ composite on the surface of BC.

The UV-Vis DRS spectra of BC, $ZnFe_2O_4$, and ZnFe/BC are displayed in Fig. 4a and revealed that the photocatalysts exhibited wide visible-light absorption capacity. Based on the Kubelka–Munk equation and the Tauc relationship (eqn (3) and (4)),[37,55,56] the band-gap energies (E_g) of BC, $ZnFe_2O_4$, and ZnFe/BC were calculated as 2.46, 1.95, and 2.16 eV, respectively, from plots of $(\alpha h\nu)^2$ *versus* energy ($h\nu$) (Fig. 4b).

$$F(R) = (1 - R^2)/2R \qquad (3)$$

$$(\alpha h\nu)^2 = A(h\nu - E_g) \qquad (4)$$

Here, R is the diffuse reflectance, $F(R)$ is the transformed reflectance according to the Kubelka–Munk equation coefficient, h is Planck's constant, ν is the frequency of the light, A is a material constant, and α is the absorption coefficient, which is equivalent to $F(R)$ numerically.

3.2. High catalytic activity and reusability of ZnFe/BC

In order to illustrate the catalytic performance of ZnFe/BC in Vis/ZnFe/BC/PMS, the degradation of SDZ was performed in various systems at natural pH (6.08). The loading of ZnFe/BC was 0.5 g L^{-1} and the SDZ concentration was 30 mg L^{-1}. The results are depicted in Fig. 5. Evidently, negligible degradation of SDZ was obtained with visible-light irradiation alone, reflecting its high stability. Direct oxidation of SDZ by PMS was also only slight due to the limited oxidizing ability of PMS ($E^0 = 1.82$ V).[57] Adsorption of SDZ on the surfaces of BC or ZnFe/BC
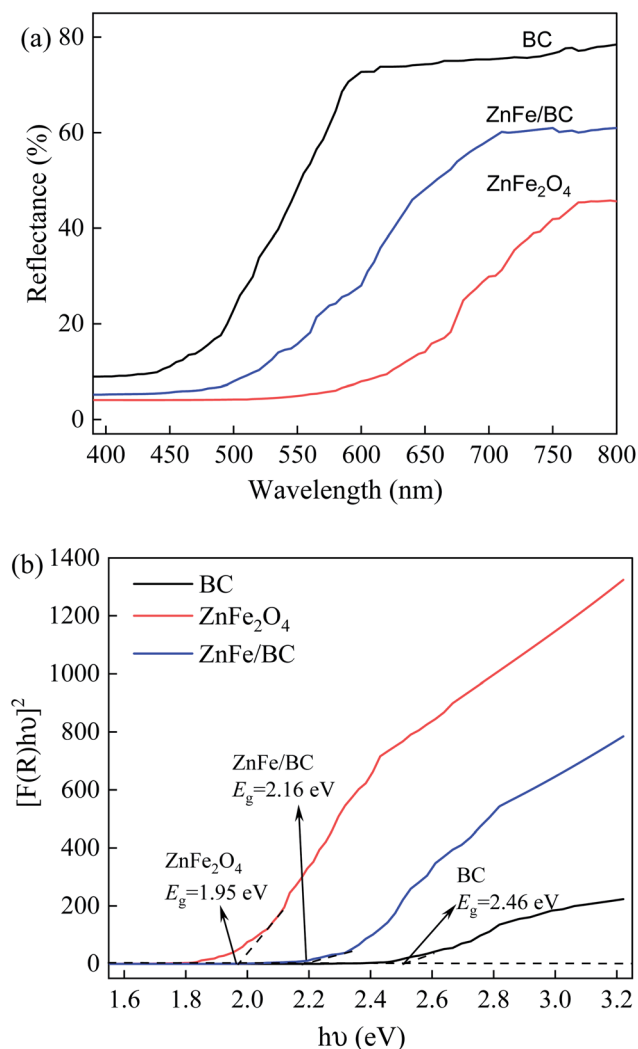

Fig. 4 UV-Vis DRS spectra of the catalyst samples (a) reflectance spectra and (b) Kubelka–Munk model of BC, $ZnFe_2O_4$ and ZnFe/BC.
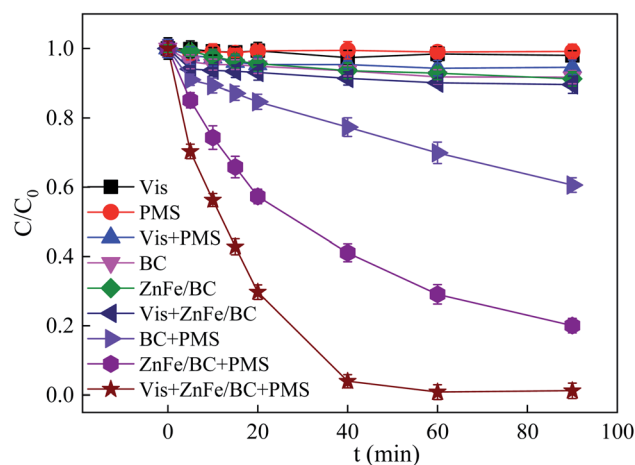

Fig. 5 Degradation of SDZ under different reaction conditions ($C_0 = 30$ mg L^{-1}, pH = 6, PMS = 5 mmol L^{-1}, ZnFe/BC = 0.5 g L^{-1}, $\lambda \geq 400$ nm).

was less than 9%. Therefore, no high catalytic activity of ZnFe/BC under visible-light irradiation was observed. Obviously, compared with pure physico-chemical adsorption, the degradation capacities were significantly enhanced in the presence of PMS. As shown in Fig. 5, the removal efficiency of SDZ was 6.42% in the Vis/PMS system, illustrating that visible-light irradiation has only weak activating ability and cannot activate PMS. Although the use of MIL-100(Fe)/ZnFe$_2$O$_4$/flake-like porous carbon nitride has been reported for the photocatalytic degradation of nonylphenol (NP) under illumination from an Xe lamp, the generation of $\cdot$O$_2{}^-$ radicals contributed to NP degradation.[58] Light from an Xe lamp was not powerful enough (350 W) to efficiently generate free radicals such as $\cdot$O$_2{}^-$, leading to an unfavorable ability to degrade SDZ. Interestingly, the removal efficiency of SDZ reached 39.6% in the BC/PMS system, suggesting that PMS was activated by BC to generate reactive oxygen species for SDZ degradation.[42,43] The composite sample showed stronger catalytic performance for PMS and the degree of decomposition was significantly improved to 80% in the ZnFe/BC/PMS system. The catalytic degradation of SDZ followed pseudo-first-order kinetics. The calculated reaction rate constants (k) are summarized in Table S1.† The SDZ degradation efficiency was significantly improved by the introduction of visible-light irradiation into the ZnFe/BC/PMS system and increased to 98.8%. Moreover, the decomposition rate constant of SDZ in the Vis/ZnFe/BC/PMS system (0.082 min^{-1}) was 3.56 times larger than that in the ZnFe/BC/PMS system (0.018 min^{-1}). This further confirmed that the synergistic interaction between ZnFe/BC and visible-light irradiation in enhancing PMS activation resulted in an obvious improvement of catalytic performance.

Recyclability and stability are important factors for practical applications. Therefore, the reusability of ZnFe/BC was assessed by monitoring the degradation of SDZ over four cycles under the same operation conditions, and the results are shown in Fig. 6a. It can be seen in Fig. 6a and b that the extents of removal of SDZ in the Vis/ZnFe/BC/PMS system over the four cycles ranged from 97.8% to 99.1%, with the leaching of Zn and Fe ions not exceeding 0.41 mg L^{-1} and 0.39 mg L^{-1}, respectively. The low leaching concentrations of Zn and Fe in the effluent are within the limits stipulated by the Discharge Standard of Pollutants for Municipal Wastewater Treatment Plant (GB18918-2002) in China. Meanwhile, the ZnFe/BC particles maintained their initial crystallinity after four cycles (Fig. 6c), indicating excellent stability and reusability.

3.3. Performance comparison of dissolved gas and reactor

The degradation of SDZ by PMS activated by ZnFe/BC under visible light (Vis) irradiation was performed in both the above-mentioned ALR and a conventional bubble column reactor (BCR; the ALR without the internal draft tube). As shown in Fig. 7, a higher degradation extent and removal of SDZ were achieved in the ALR compared to those in the conventional BCR. The degree of degradation and removal rate of SDZ in the ALR were 98.8% and 0.082 min^{-1}, respectively, as compared to 85.9% and 0.030 min^{-1} in the BCR. Compared with the BCR,
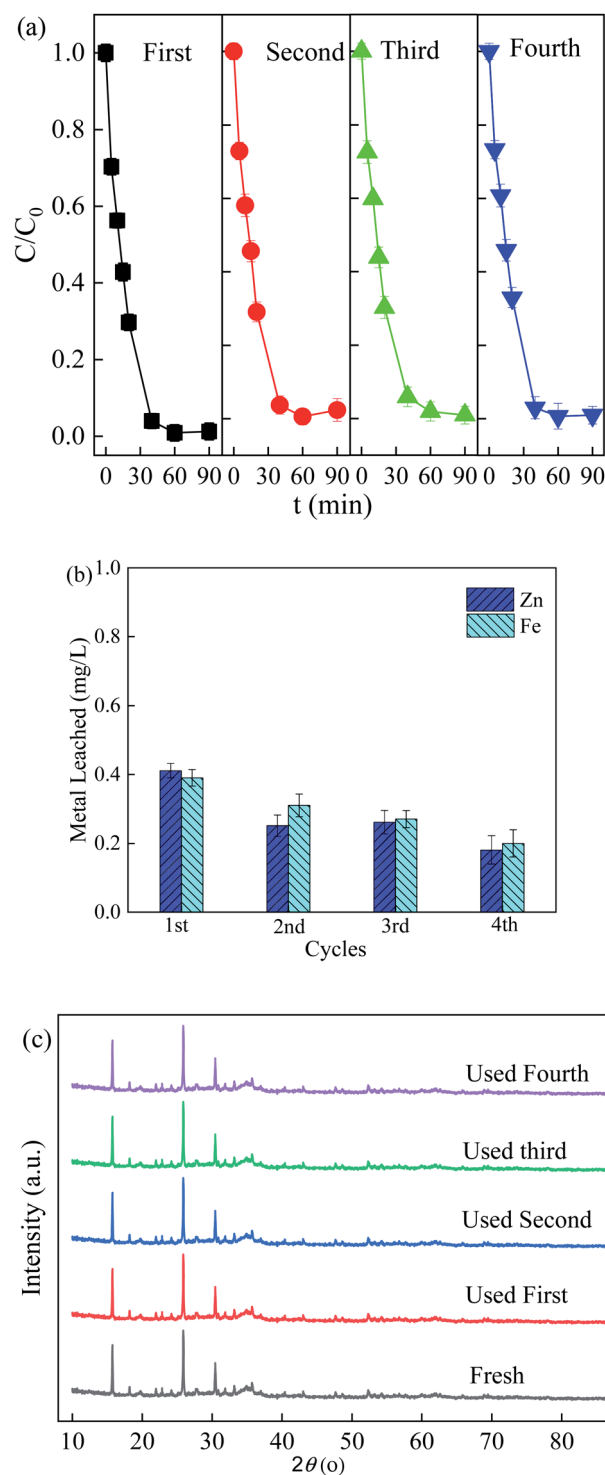

Fig. 6 (a) Reusability of ZnFe/BC in the Vis/ZnFe/BC/PMS system (C_0 = 30 mg L^{-1}, pH = 6, PMS = 5 mmol L^{-1}, ZnFe/BC = 0.5 g L^{-1}, $\lambda \geq$ 400 nm); (b) content of metal elements in the leaching solutions; (c) XRD patterns of fresh and used ZnFe/BC.

the ALR with an internal draft tube allowed for smooth and steady circulation of the catalyst particles in the reactor, which favored extensive contact between the reactants as well as high mass- and heat-transfer rates. Therefore, the ALR was used in subsequent experiments due to its superior performance.
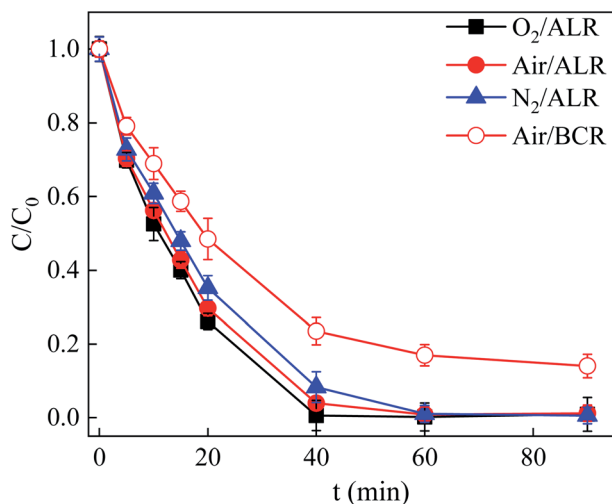
Fig. 7 Effect of dissolved gas on SDZ degradation in ALR and BCR (C_0 = 30 mg L^{-1}, pH = 6, PMS = 5 mmol L^{-1}, ZnFe/BC = 0.5 g L^{-1}, $\lambda \geq 400$ nm).

Some studies have shown that superoxide free radical ($^{\bullet}O_2^{-}$) is generated through electron transfer to dissolved O_2.[59,60] Thus, experiments in different atmospheres (N_2, O_2, and air) were carried out to confirm the existence and contribution of $^{\bullet}O_2^{-}$ in the Vis/ZnFe/BC/PMS system. The role of O_2 in the degradation of SDZ was investigated by bubbling N_2 or O_2 instead of air in the Vis/ZnFe/BC/PMS system. As indicated in Fig. 7, the degradation efficiency of SDZ decreased from 98.8% to 88.0% and the degradation rate decreased from 0.082 min^{-1} to 0.075 min^{-1} when air was replaced by N_2, presumably because less $^{\bullet}O_2^{-}$ was formed.[61] The SDZ degradation efficiency and removal rate increased to 99.1% and 0.115 min^{-1}, respectively, when air was replaced by pure O_2 such that there was more dissolved O_2 and hence more $^{\bullet}O_2^{-}$.[61]

3.4. Effects of operating parameters

Considering practical application of the Vis/ZnFe/BC/PMS system, the effects of ZnFe/BC dosage, PMS dosage, and initial pH on SDZ degradation were studied, and the results are shown in Fig. 8. It can be seen from Fig. 8a that the degradation efficiency of SDZ was obviously increased from 40.2% to 98.8% with increasing PMS dosage from 1 to 5 mmol L^{-1} at 30 mg L^{-1} SDZ concentration, natural initial pH 6.0, and 0.5 g L^{-1} ZnFe/BC. This implied that increased amount of oxidant was directly correlated with the quantities of reactive radicals produced by its decomposition. However, when the PMS concentration was further increased to 7 mmol L^{-1}, the SDZ degradation efficiency and rate tended to saturation. The active sites of ZnFe/BC at 0.5 g L^{-1} addition were occupied by 5 mmol L^{-1} PMS and the limited activation ability of Vis could not significantly enhance the degradation of SDZ. No further sites were available when the PMS concentration was increased to 7 mmol L^{-1}. A similar phenomenon was reported by Fan and co-workers when employing PMS activated by a sewage sludge biochar-based catalyst to degrade bisphenol A.[43]

SDZ removal rates at various ZnFe/BC dosages were investigated (Fig. 8b) at 5 mmol L^{-1} PMS, 30 mg L^{-1} SDZ, and initial pH 6. For increasing ZnFe/BC loadings of 0.1, 0.3, 0.5, and 0.7 g L^{-1}, the SDZ degradation efficiency and rate constant increased from 79.5% to 99.4% and from 0.013 min^{-1} to 0.091 min^{-1}, respectively. A higher dosage of catalyst provides more active sites for PMS activation and SDZ degradation.

The influence of varying pH_0 from 3 to 10 was examined using the Vis/ZnFe/BC/PMS system for SDZ degradation (Fig. 8c). SDZ degradation efficiencies remained similar over a wide pH range. When the pH_0 was increased from 3 to 10, the rate constant decreased significantly from 0.084 to 0.069 min^{-1}, while the degradation efficiency in 90 min changed very slightly from 99.0% to 99.4%. The promising removal results demonstrated that the ZnFe/BC catalyst may be applied over a wide range of initial pH (3–10) for the activation of PMS under visible-light irradiation.

3.5. Reaction mechanism

In order to delineate the photocatalytic reaction mechanism, a series of radical quenching experiments was conducted to ascertain the main active species. The scavengers EtOH, TBA, BQ, NaN$_3$, K$_2$Cr$_2$O$_7$, and EDTA were employed to quench SO$_4^{\bullet-}$ and $^{\bullet}$OH, $^{\bullet}$OH, $^{\bullet}O_2^{-}$, $^1O_2$, e^{-}, and h^{+}, respectively. As shown in Fig. 9, the SDZ degradation rate in the presence of TBA decreased from 0.082 to 0.058 min^{-1}, suggesting that $^{\bullet}$OH played a limited role in the process. Similarly to TBA, when EtOH, as a quencher of both SO$_4^{\bullet-}$ and $^{\bullet}$OH, was added to the reaction solution, the SDZ removal rate decreased to 0.038 min^{-1}, implying that both SO$_4^{\bullet-}$ and $^{\bullet}$OH were generated in the Vis/ZnFe/BC/PMS system. However, adding excess EtOH or TBA did not fully suppress SDZ removal, demonstrating that other active oxygen species were also operative in the reaction solution. Moreover, previous literature reports have indicated that $^{\bullet}O_2^{-}$ may be generated during the PMS activation process.[37,62,63] Therefore, BQ was selected to verify the involvement of $^{\bullet}O_2^{-}$ due to the high rate constant of their reaction ($k_{O_2^{-}} = 2.9 \times 10^9$ m^{-1} s^{-1}).[62] Indeed, when BQ was introduced, the SDZ degradation rate decreased significantly to 0.028 min^{-1}, suggesting that $^{\bullet}O_2^{-}$ played an important role in the process. In addition, $^1O_2$ also contributed to the degradation of SDZ, as proved by the addition of NaN$_3$. Clearly, the introduction of NaN$_3$ had a suppressing effect on the degradation of SDZ, revealing that $^1O_2$ also has a notable impact in the Vis/ZnFe/BC/PMS system. The elimination rate of SDZ decreased from 0.082 to 0.036 min^{-1}. Besides, EDTA and K$_2$Cr$_2$O$_7$ are widely utilized to investigate the presence of photogenerated h^{+} and e^{-}, respectively. As shown in Fig. 9, the SDZ degradation efficiency decreased from 98.78% to 80.85% and 83.6%, while the rate constant decreased from 0.082 min^{-1} to 0.022 min^{-1} and 0.029 min^{-1}, when EDTA and K$_2$Cr$_2$O$_7$ were added, respectively, revealing that both h^{+} and e^{-} played important roles in the degradation of SDZ.

To further confirm the reactive species involved in the degradation of SDZ in the Vis/ZnFe/BC/PMS system, EPR measurements were carried out in the presence of DMPO and
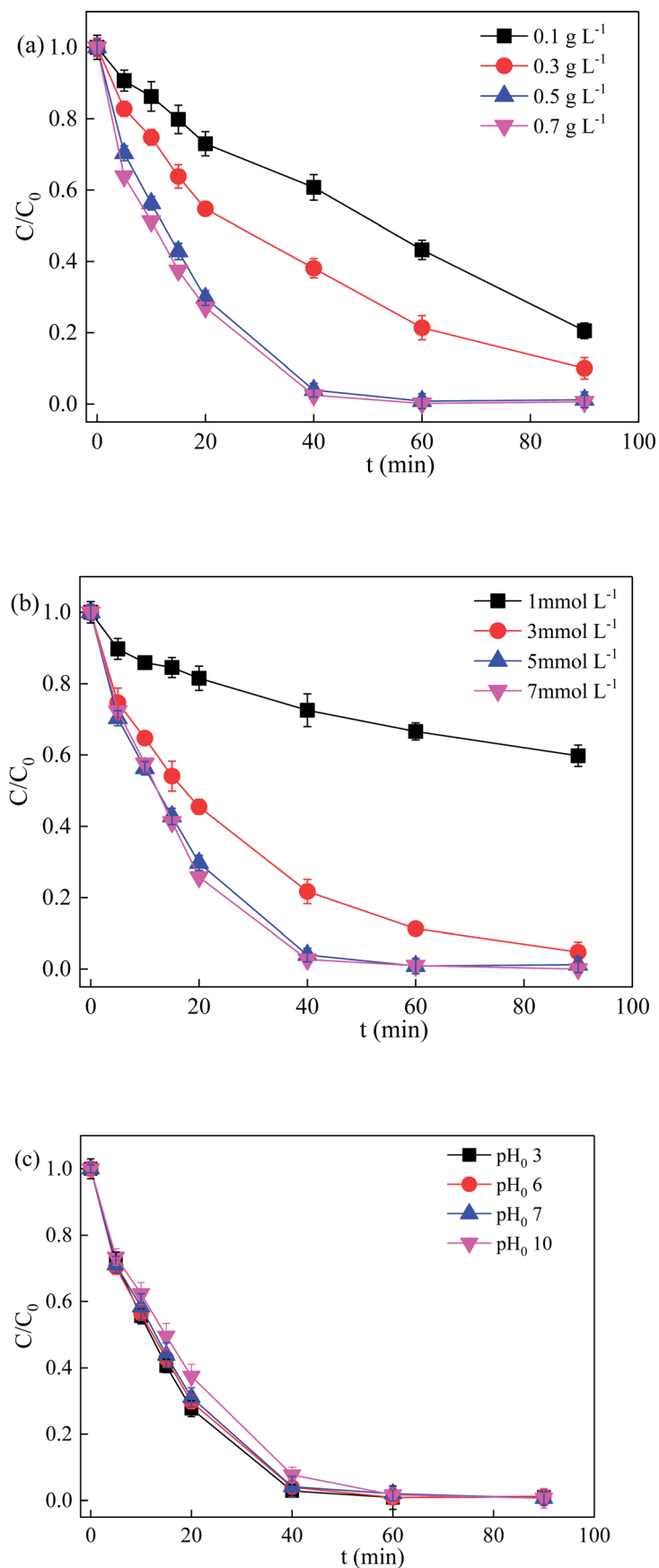
Fig. 8 Effect of reaction conditions for the degradation of SDZ: (a) catalyst dosage, (b) PMS concentration, and (c) initial pH_0 ($C_0 = 30$ mg L^{-1}, pH = 6, PMS = 5 mmol L^{-1}, ZnFe/BC = 0.5 g L^{-1}, $\lambda \geq 400$ nm).

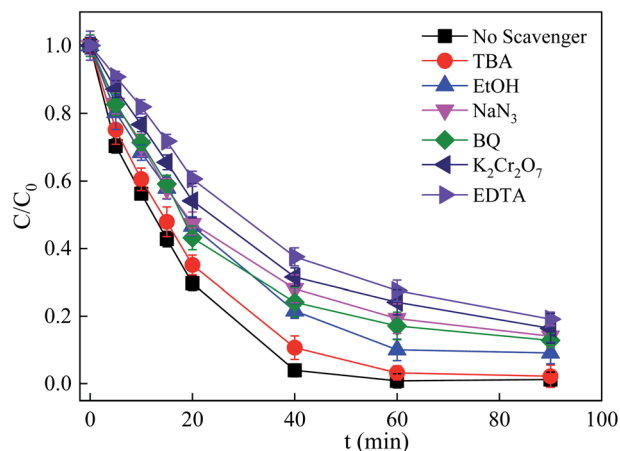**Fig. 9** Effect of radical scavengers on the degradation of SDZ ($C_0 = 30$ mg L^{-1}, pH = 6, PMS = 5 mmol L^{-1}, ZnFe/BC = 0.5 g L^{-1}, $C_{TBA} = C_{EtOH} = 100$ mmol L^{-1}, $C_{BQ} = C_{NaN_3} = C_{K_2Cr_2O_7} = C_{EDTA} = 10$ mmol L^{-1}, $\lambda \geq 400$ nm).

TMP, and the results are shown in Fig. 10. It can be seen from Fig. 10a that strong $1:2:2:1$ quartet and $1:1:1:1:1:1$ sextet characteristic signals in the combination systems (such as BC/PMS, ZnFe/BC/PMS, and Vis/ZnFe/BC/PMS) were detected due to DMPO adduct formation, confirming the presence of $^{\bullet}$OH and SO$_4^{\bullet-}$. However, only low-intensity signals were observed in Vis/PMS system because of low catalytic capacity of Vis for PMS. Compared with the combination systems, these peaks were inconspicuous in only PMS, illustrating that $^{\bullet}$OH and SO$_4^{\bullet-}$ could not be generated through the self-decomposition of PMS. Meanwhile, a significant triplet signal of ^{1}O$_2$ ($1:1:1$ ratio) could be seen from Fig. 10b in the presence of TMP as a spin-trapping agent, which implies that abundant ^{1}O$_2$ was generated in the BC/PMS, ZnFe/BC/PMS, and Vis/ZnFe/BC/PMS system. Similarly, the triplet signal of ^{1}O$_2$ was weak in Vis/PMS, while it was inconspicuous in only PMS. This further revealed that ^{1}O$_2$ could been produced via activating PMS by BC, ZnFe/BC, and the combination of ZnFe/BC and Vis.

The energy band positions of ZnFe$_2$O$_4$ and BC were investigated in order to obtain deeper insight into the photocatalytic mechanism. Mott–Schottky analysis was employed with an initial frequency of 1000 Hz, and the results are shown in Fig. 11a. By extrapolating the graph to $1/C^2 = 0$, the slope of the plot intercepts the x-axis at the flat band potential (E_{fb}), where E_{fb} is roughly equal to the band energy for most semiconductors. Moreover, a positive slope indicates the conduction band (CB) potential (E_{CB}) for an n-type semiconductor, whereas a negative slope indicates the valence band (VB) potential (E_{VB}) for a p-type semiconductor.[56] In this way, the CB energy of ZnFe$_2$O$_4$ was obtained as 2.35 eV and the VB energy of BC was obtained as -0.73 eV with respect to Ag/AgCl. According to the UV/Vis DRS analysis results, the E_{VB} of ZnFe$_2$O$_4$ and the E_{CB} of BC were calculated according to the following formula[56,64,65] as 0.40 eV and 1.73 eV, respectively.

$$E_{VB} = E_{CB} + E_g \quad (5)$$

Based on the above discussion and analysis, a preliminary photocatalytic degradation mechanism for SDZ by PMS activated by ZnFe/BC under visible light may be proposed, as shown in Fig. 11b. BC showed excellent catalytic ability towards PMS due to its abundant oxygenated functional groups, which serve to effectively generate ^{1}O$_2$, $^{\bullet}$OH, and SO$_4^{\bullet-}$.[66–68] ZnFe/BC was excited under visible-light irradiation to produce e$^-$$_{TEL}$ and h$^+$ (eqn (6)). Photogenerated e$^-$$_{TEL}$ in BC were captured by adsorbed O$_2$ to produce $^{\bullet}$O$_2^-$ according to eqn (7),[59,60] owing to its more negative CB than that of O$_2$/$^{\bullet}$O$_2^-$ (-0.33 eV).[69,70] The photogenerated e$^-$ could easily migrate from the CB of ZnFe$_2$O$_4$ to the h$^+$ in the VB of BC and recombine with them. Moreover, the h$^+$ in ZnFe$_2$O$_4$ showed strong oxidizing ability and could directly degrade pollutants, and could also activate PMS to generate SO$_5^{\bullet-}$ according to eqn (8).[37] Both the self-reaction of SO$_5^{\bullet-}$ and the reaction between $^{\bullet}$O$_2^-$ and $^{\bullet}$OH (eqn (9) and (10)) could
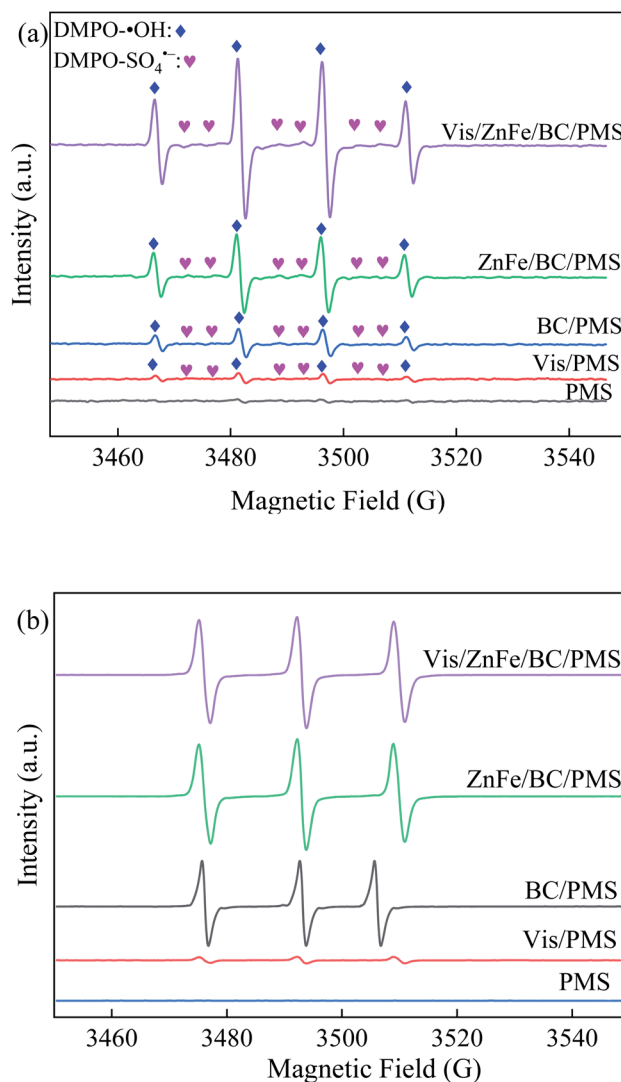
Fig. 10 ESR spectra of (a) DMPO-$^{\bullet}$OH and DMPO-SO$_4^{\bullet-}$$_{TEL}$, (b) TMP-^{1}O$_2$ signals in PMS, Vis/PMS, BC/PMS, ZnFe/BC/PMS, and Vis/ZnFe/BC/PMS systems ($C_{DMPO} = 10$ mg L^{-1}, $C_{TMP} = 10$ mg L^{-1}, pH = 6, PMS = 5 mmol L^{-1}, ZnFe/BC = 0.5 g L^{-1}).

generate $^1O_2$.[37] The photogenerated e^{TEL}, h^+, $\cdot O_2^-$, $^1O_2$, $SO_4^{\cdot-}$, and $\cdot OH$ reacted with SDZ through free radical and non-radical pathways to produce intermediates, achieving its efficient removal (eqn (11)).

$$ZnFe/BC + h\nu \rightarrow ZnFe/BC\ (e^- + h^+) \tag{6}$$

$$O_2 + e^- \rightarrow \cdot O_2^- \tag{7}$$

$$HSO_5^- + h^+ \rightarrow SO_5^{\cdot-} + H^+ \tag{8}$$

$$SO_5^{\cdot-} + SO_5^{\cdot-} \rightarrow 2SO_4^{\cdot-} + {}^1O_2 \tag{9}$$

$$\cdot O_2^- + \cdot OH \rightarrow OH^- + {}^1O_2 \tag{10}$$

$$e^-/h^+/{}^1O_2/\cdot O_2^-/\cdot OH/SO_4^{\cdot-} + SDZ \rightarrow intermediates \tag{11}$$
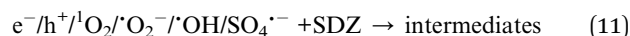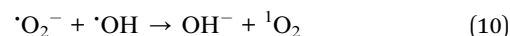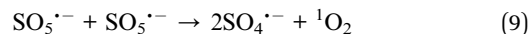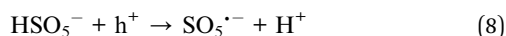
3.6. TOC and toxicity evaluation of effluent

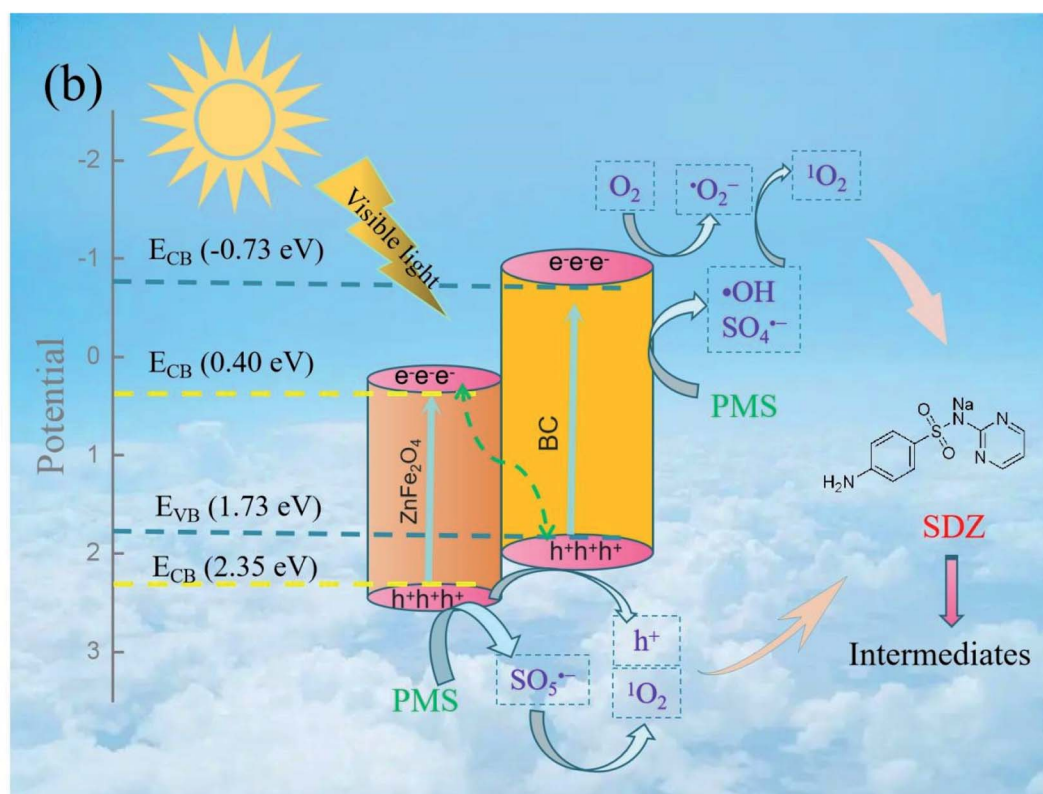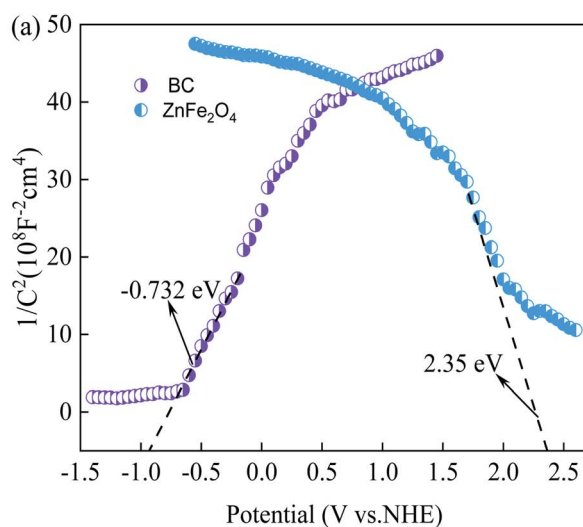Complete degradation of SDZ does not mean that it was completely oxidized to harmless small molecules, such as CO_2,

Fig. 11 (a) Mott–Schottky plots of $ZnFe_2O_4$ and BC and (b) The possible removal mechanism of SDZ by Vis/ZnFe/BC/PMS system.
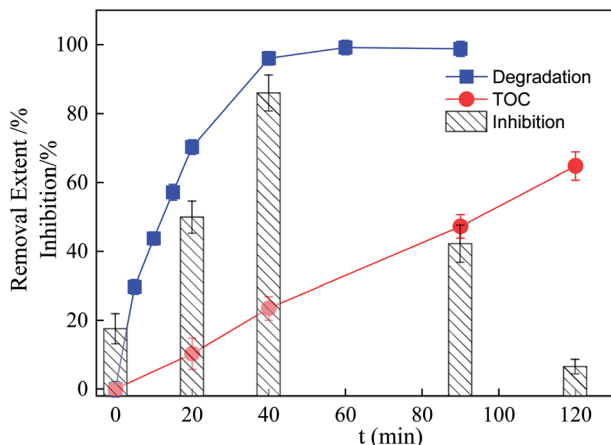
View Article Online

RSC Advances

Paper

Open Access Article. Published on 24 August 2022. Downloaded on 2/11/2026 8:00:05 PM.
This article is licensed under a Creative Commons Attribution-NonCommercial 3.0 Unported Licence.

Fig. 12 Changes of acute toxicity and TOC removal during SDZ degradation process (C_0 = 30 mg L^{-1}, pH = 6, PMS = 5 mmol L^{-1}, ZnFe/BC = 0.5 g L^{-1}, $\lambda \geq$ 400 nm).

H_2O, and NO_3^-, but the TOC removal gives a measure of the mineralization degree of organic pollutants in AOPs.[71,72] Thus, the TOC removal of the SDZ solution was explored, and the results are shown in Fig. 12. The extent of SDZ degradation reached 96.05% after 40 min of reaction, but the TOC removal was less than 24%. On further extending the treatment to 2 h, the TOC removal efficiency displayed a satisfactory result (approximately 64.8%), revealing that recalcitrant intermediates were formed.

Compared to the parent compound, more toxic intermediates are usually produced during the photocatalytic treatment of antibiotics.[73–75] Thus, the acute toxicity was investigated towards luminescent bacteria, and the results are shown in Fig. 12. It can be seen from Fig. 12 that the luminescence inhibition ratio increased from 17.43% to 85.97% within the first 40 min, proving that some toxic intermediates were produced at the beginning of the reaction. The luminescence inhibition ratio then decreased sharply to just 6.41% at 120 min, demonstrating that SDZ and its intermediates had been significantly decomposed into low/nontoxic compounds by the Vis/ZnFe/BC/PMS system. Hence, the present system could be described as ecotoxicologically safe.

4. Conclusion

$ZnFe_2O_4$ has been combined with BC to form ZnFe/BC and ZnFe/BC was applied as an efficient PMS activator to achieve efficient SDZ elimination under visible light irradiation in an internal loop-lift reactor. The photocatalytic performance of ZnFe/BC has been assessed on the basis of its structure, activity, stability, and reusability towards SDZ in the visible-light-induced process. The catalyst displayed excellent degradation performance, and EPR and chemical quenching tests revealed that e$^-$, h$^+$, $^1O_2$, $\cdot O_2^-$, $\cdot OH$, and $SO_4^{\cdot-}$ were responsible for the removal of SDZ. The Vis/ZnFe/BC/PMS system is efficient over a wide pH range. In addition, the mineralization rate of SDZ and biotoxicity be considered before practical applications. The TOC

removal only reached 64.8% after 2 h reaction, but the acute toxicity of the effluent achieved the satisfactory effect. The acute toxicity of the effluent during the SDZ degradation process first increased to 85.97% after 40 min of reaction, but then gradually decreased to 6.41%. In summary, the findings of this study provide a novel method for enhancing the photo-catalytic effect of ZnFe/BC in PMS activation systems. Moreover, the development of ZnFe/BC constituted an effective method for solid waste resource utilization and the remediation of antibiotic-contaminated wastewater.

Author contributions

Yan Wang: Investigation, Methodology, Data curation, Formal analysis, Visualization, Writing – original draft, Writing – review & editing, Supervision. Tao Gan: Investigation, Data curation. Jingyu Xiu: Investigation, Data curation. Ganghua Liu: Conceptualization, Data curation, Methodology. Haiming Zou: Formal analysis, Funding acquisition, Supervision.

Conflicts of interest

There are no conflicts to declare.

Acknowledgements

This study was supported by the Natural Science Foundation of Anhui Province (No. 1808085MB49, 2008085ME169, 2108085MD140, 2108085QB56), in China; Innovation and Entrepreneurship Training Program for College Students in Anhui Province (S202110879254, S202110879251).

References

1 J. C. Serna-Carrizales, V. H. Collins-Martínez, E. Flórez, C. F. A. Gomez-Duran, G. Palestino and R. Ocampo-Pérez, J. Mol. Liq., 2021, 324, 114740.
2 Y. Liu, X. Zhang, J. Deng and Y. Liu, Chemosphere, 2021, 277, 130305.
3 F. Zhu, J. Pan, Q. Zou, M. Wu, H. Wang and G. Xu, Chemosphere, 2021, 274, 129713.
4 L. Zhu, Z. Shi, L. Deng and Y. Duan, Colloids Surf., A, 2021, 609, 125637.
5 W. Yang, P. Hong, D. Yang, Y. Yang, Z. Wu, C. Xie, J. He, K. Zhang, L. Kong and J. Liu, J. Colloid Interface Sci., 2021, 597, 56–65.
6 H. Cui, Y. Tian, J. Zhang, S. Ma, L. Li, W. Zuo, L. Zhang and T. Wang, Chem. Eng. J., 2021, 417, 128152.
7 Z. Y. Lu, Y. L. Ma, J. T. Zhang, N. S. Fan, B. C. Huang and R. C. Jin, J. Water Proc. Eng., 2020, 38, 101681.
8 M. Wang, C. Jin, J. Kang, J. Liu, Y. Tang, Z. Li and S. Li, Chem. Eng. J., 2021, 416, 128118.
9 W. Wang, M. Chen, D. Wang, M. Yan and Z. Liu, Sci. Total Environ., 2021, 772, 145522.
10 T. Zhang, Y. Yang, X. Li, H. Yu, N. Wang, H. Li, P. Du, Y. Jiang, X. Fan and Z. Zhou, Sep. Purif. Technol., 2020, 239, 116537.

24098 | RSC Adv., 2022, 12, 24088–24100

© 2022 The Author(s). Published by the Royal Society of Chemistry

11 W. Guo, Q. Zhao, J. Du, H. Wang, X. Li and N. Ren, *Chem. Eng. J.*, 2020, **388**, 124303.

12 A. Shabanloo, M. Salari, N. Shabanloo, M. H. Dehghani, C. U. Pittman and D. Mohan, *J. Mol. Liq.*, 2020, **298**, 112088.

13 S. Xiao, M. Cheng, H. Zhong, Z. Liu, Y. Liu, X. Yang and Q. Liang, *Chem. Eng. J.*, 2020, **384**, 123265.

14 Y. Lei, J. Lu, M. Zhu, J. Xie, S. Peng and C. Zhu, *Chem. Eng. J.*, 2020, **379**, 122339.

15 J. Zhang, H. Song, Y. Liu, L. Wang, D. Li, C. Liu, M. Gong, Z. Zhang, T. Yang and J. Ma, *Sep. Purif. Technol.*, 2019, **224**, 142–151.

16 Z. Lin, W. Qin, L. Sun, X. Yuan and D. Xia, *J. Water Process Eng.*, 2020, **38**, 101636.

17 Y. Qi, R. Qu, J. Liu, J. Chen, G. Al-Basher, N. Alsultan, Z. Wang and Z. Huo, *Chemosphere*, 2019, **237**, 124484.

18 X. Zhang, Z. Chen, J. Kang, S. Zhao, B. Wang, P. Yan, F. Deng, J. Shen and W. Chu, *J. Hazard. Mater.*, 2021, **401**, 123837.

19 H. Milh, D. Cabooter and R. Dewil, *Chem. Eng. J.*, 2021, **422**, 130457.

20 Y. Nie, H. Zhou, S. Tian, X. Tian, C. Yang, Y. Li, Y. Tian and Y. Wang, *Chem. Eng. J.*, 2022, **427**, 130998.

21 H. Fu, S. Ma, P. Zhao, S. Xu and S. Zhan, *Chem. Eng. J.*, 2019, **360**, 157–170.

22 H. L. So, K. Y. Lin, W. Chu and H. Gong, *Ind. Eng. Chem. Res.*, 2020, **59**, 4257–4264.

23 B.-M. Jun, S. S. Elanchezhiyan, Y. Yoon, D. Wang, S. Kim, S. Muthu Prabhu and C. M. Park, *Chem. Eng. J.*, 2020, **393**, 124733.

24 J. Wang, J. Cai, S. Wang, X. Zhou, X. Ding, J. Ali, L. Zheng, S. Wang, L. Yang, S. Xi, M. Wang and Z. Chen, *Chem. Eng. J.*, 2022, **428**, 131233.

25 Y. Yu, N. Li, X. Lu, B. Yan, G. Chen, Y. Wang, X. Duan, Z. Cheng and S. Wang, *J. Hazard. Mater.*, 2021, **421**, 126735.

26 S. Wang, L. Xu and J. Wang, *Chem. Eng. J.*, 2022, **428**, 131066.

27 Y. Wang, Y. Song, N. Li, W. Liu, B. Yan, Y. Yu, L. Liang, G. Chen, L. a. Hou and S. Wang, *J. Hazard. Mater.*, 2022, **421**, 126794.

28 Z. Zhang, X. Huang, J. Ma, Z. Pei, X. Luo, L. Ke, F. Qin, Y. Li, R. Yang, Y. Zhu and Q. Zhang, *Water Res.*, 2021, **201**, 117288.

29 H. Zhang, Y. Song, L. C. Nengzi, J. Gou, B. Li and X. Cheng, *Chem. Eng. J.*, 2020, **379**, 122362.

30 A. Eslami, M. Hashemi and F. Ghanbari, *J. Clean. Prod.*, 2018, **195**, 1389–1397.

31 D. Roy, S. Neogi and S. De, *Chem. Eng. J.*, 2022, **428**, 131028.

32 B. Joshi, E. Samuel, C. Park, Y. Kim, H. S. Lee and S. S. Yoon, *Appl. Surf. Sci.*, 2021, **559**, 149951.

33 J. Feng, P. Nian, L. Peng, A. Zhang and Y. Sun, *Chemosphere*, 2021, **271**, 129575.

34 K. Shetty, L. Renuka, H. P. Nagaswarupa, H. Nagabhushana, K. S. Anantharaju, D. Rangappa, S. C. Prashantha and K. Ashwini, *Mater. Today Proc.*, 2017, **4**, 11806–11815.

35 Y. L. Yan, Q. J. Fang, J. K. Pan, J. Yang, L.-l. Zhang, W. Zhang, G.-l. Zhuang, X. Zhong, S. W. Deng and J. G. Wang, *Chem. Eng. J.*, 2021, **408**, 127358.

36 S. S. Sonu, V. Dutta, P. Raizada, A. Hosseini-Bandegharaei, V. Thakur, V. H. Nguyen, Q. VanLe and P. Singh, *J. Environ. Chem. Eng.*, 2021, **9**, 105812.

37 H. Tang, R. Li, X. Fan, Y. Xu, H. Lin and H. Zhang, *J. Environ. Chem. Eng.*, 2022, **10**, 107797.

38 A. Behera and K. Parida, *Mater. Today Proc.*, 2021, **35**, 203–206.

39 C. Zheng, C. Zhang, K. Zhang, J. Zhang, L. Jin, A. M. Asiri, K. A. Alamry, L. He and X. Chu, *Sens. Actuators, B*, 2021, **330**, 129280.

40 J. Ding, W. Xu, S. Liu, Y. Liu, X. Tan, X. Li, Z. Li, P. Zhang, L. Du and M. Li, *J. Colloid Interface Sci.*, 2021, **588**, 776–786.

41 L. Chen, X. Jiang, R. Xie, Y. Zhang, Y. Jin and W. Jiang, *Sep. Purif. Technol.*, 2020, **250**, 117232.

42 Y. Zhao, X. Yuan, X. Li, L. Jiang and H. Wang, *J. Hazard. Mater.*, 2021, **409**, 124893.

43 X. Fan, H. Lin, J. Zhao, Y. Mao, J. Zhang and H. Zhang, *Sep. Purif. Technol.*, 2021, **272**, 118909.

44 S. M. Teli and C. S. Mathpati, *Chin. J. Chem. Eng.*, 2021, **32**, 39–60.

45 J. Tao, J. Huang, S. Geng, F. Gao, T. He and Q. Huang, *Chem. Eng. J.*, 2020, **386**, 122769.

46 A. Makofane, D. E. Motaung and N. C. Hintsho-Mbita, *Ceram. Int.*, 2021, **47**, 22615–22626.

47 X. Rong, H. Chen, J. Rong, X. Zhang, J. Wei, S. Liu, X. Zhou, J. Xu, F. Qiu and Z. Wu, *Chem. Eng. J.*, 2019, **371**, 286–293.

48 Y. Wang, R. Priambodo, H. Zhang and Y.-H. Huang, *RSC Adv.*, 2015, **5**, 45276–45283.

49 A. J. Santos, I. Sirés and E. Brillas, *Chemosphere*, 2021, **263**, 128271.

50 X. Zhu, C. Cao, S. Su, A. Xia, H. Zhang, H. Li, Z. Liu and C. Jin, *Ceram. Int.*, 2021, **47**, 15173–15179.

51 A. S. Basaleh, *J. Mater. Res. Technol.*, 2021, **11**, 1260–1271.

52 S. Li, Y. Zhang, L. Han, X. Li and Y. Xu, *Sens. Actuators, B*, 2021, **344**, 130251.

53 S. Krishnan, S. Murugesan, V. Vasanthakumar, A. Priyadharsan, M. Alsawalha, T. Alomayri and B. Yuan, *Colloids Surf., A*, 2021, **611**, 125835.

54 K. K. Das, L. Paramanik and K. Parida, *Int. J. Hydrogen Energy*, 2021, **46**, 24484–24500.

55 F. G. El Desouky, M. M. Saadeldin, M. A. Mahdy and I. K. El Zawawi, *Vacuum*, 2021, **185**, 110003.

56 R. Li, H. Hu, Y. Ma, X. Liu, L. Zhang, S. Zhou, B. Deng, H. Lin and H. Zhang, *J. Clean. Prod.*, 2020, **276**, 124246.

57 W. V. Steele and E. H. Appelman, *J. Chem. Thermodyn.*, 1982, **14**, 337–344.

58 G. Zeng, R. Yang, X. Fu, Z. Zhou, Z. Xu, Z. Zhou, Z. Qiu, Q. Sui and S. Lyu, *Sep. Purif. Technol.*, 2021, **264**, 118441.

59 K. Zhang, P. Sun, A. Khan and Y. Zhang, *Sci. Total Environ.*, 2021, **765**, 144630.

60 N. Welter, J. Leichtweis, S. Silvestri, P. I. Z. Sánchez, A. C. C. Mejía and E. Carissimi, *J. Alloys Compd.*, 2022, **901**, 163758.

61 S. Renukadevi and A. Pricilla Jeyakumari, *Inorg. Chem. Commun.*, 2020, **118**, 108047.

62 A. Khan, K. Zhang, A. K. A. Taraqqi, X. Wang, Y. Chen and Y. Zhang, *J. Colloid Interface Sci.*, 2021, **599**, 805–818.

63 Y. Wang, L. Ding, C. Liu, Y. Lu, Q. Wu, C. Wang and Q. Hu, *Sep. Purif. Technol.*, 2022, **283**, 120164.

64 K. Wang, S. Zhan, D. Zhang, H. Sun, X. Jin and J. Wang, *Colloids Surf., A*, 2021, **618**, 126362.

65 B. Zhu, H. Cheng, J. Ma, Y. Kong and S. Komarneni, *Chemosphere*, 2019, **237**, 124547.

66 Z. Feng, B. Zhou, R. Yuan, H. Li, P. He, F. Wang, Z. Chen and H. Chen, *Chem. Eng. J.*, 2022, **440**, 135669.

67 Q. Fang, S. Ye, H. Yang, K. Yang, J. Zhou, Y. Gao, Q. Lin, X. Tan and Z. Yang, *J. Hazard. Mater.*, 2021, **420**, 126569.

68 H. Luo, H. Fu, H. Yin and Q. Lin, *J. Hazard. Mater.*, 2022, **426**, 128044.

69 K. Xu, L. Jiao, C. Wang, Y. Bu, Y. Tang, L. Qiu, Q. Zhang and L. Wang, *J. Environ. Sci.*, 2022, **111**, 93–103.

70 H. Peng, Y. Li, J. Wen and X. Zheng, *Ind. Crops Prod.*, 2021, **172**, 114066.

71 K. Zhu, Q. Bin, Y. Shen, J. Huang, D. He and W. Chen, *Chem. Eng. J.*, 2020, **402**, 126090.

72 L. Guo, J. Zhao, L. Zhao, Y. Tang, J. Zhou and B. Shi, *Chem. Eng. J.*, 2021, **420**, 127698.

73 E. Evgenidou, Z. Chatzisalata, A. Tsevis, K. Bourikas, P. Torounidou, D. Sergelidis, A. Koltsakidou and D. A. Lambropoulou, *J. Environ. Chem. Eng.*, 2021, **9**, 105295.

74 H. B. Truong, B. T. Huy, S. K. Ray, G. Gyawali, Y. I. Lee, J. Cho and J. Hur, *Chemosphere*, 2022, **299**, 134320.

75 Y. Sun, R. Xiong, J. Zhang, Y. Ma, Y. Li, W. Ji, Y. Ma and Z. Wang, *Sep. Purif. Technol.*, 2022, **293**, 121066.